Journal of Southeast University (English Edition) Vol. 21, No. 2, pp. 170 - 174 June 2005 ISSN 1003—7985

Surface edge element method for 3-D electromagnetic computation

Yu Haitao

(Department of Electrical Engineering, Southeast University, Nanjing 210096, China)

Abstract: A surface edge element method is proposed and implemented in the study of electromagnetic scattering fields of general targets. The basis functions for surfaces of arbitrary shape are derived according to the geometrical properties of each triangular patch. The proposed basis functions are 3-D linear functions and the tangential components of the vectors are continuous as the traditional edge element method. Combined field integral equations (CFIE) that include both electrical field and magnetic field integral equations are used to model the electromagnetic scattering of general dielectric targets. Special treatment for singularity is presented to enhance the quality of numerical solutions. The proposed method is used to compute the scattering fields from various targets. Numerical results obtained by the proposed method are validated by results from other numerical methods.

Key words: surface edge element method; method of moment; combined field integral equations; scattering field

Method of moment (MoM) for surfaces of general targets[1] has been widely used in the studies of electromagnetics at high and low frequencies. The Rao-Wilton-Glisson (RWG) functions are constituted within pairs of adjacent triangular patches as the local elements to yield a current representation that does not have line or point charges at sub-domain boundaries. RWG to expand both electric and magnetic currents is used to compute a dielectric-resonator[2-4]. Zhang et al.[5] solved a low-frequency breakdown problem using MoM with RWG. Sarkar et al.[6] analyzed transient scattering from composite complex structures of arbitrary shapes. However, only the information on submeshes and their related medium parameters are available when the computational geometry is subdivided into triangular patches using commercial software. Thus there is no information on the adjacent triangles for deriving the RWG functions that constitute a local matrix. Consequently, one needs to search and store the data of the neighboring triangular patches, rather than just the patch itself, after the mesh generation.

An edge element method[7] was proposed by Nedelec in 1980. Like the nodal-based finite element model (FEM), the edge element method (EEM) is only involved in a local element, such as a tetrahedron in 3-D computations. Bossavit[8] has implemented it to discretize the FEM formulation for eddy current problems at low frequency and Ahn et al.[9] computed the scattering field using finite element-boundary element (FE-BE) with edge element. This method allows vector fields to be used directly as variables since only the tangential component on adjacent elements is constrained to be continuous. However, EEM is only exploited in the integral equation for specific target shapes, such as a rectangle[10]. The surface basis functions of EEM in Ref. [9] was presented for the FE-BE computations but the most important parameter, the corresponding nodal basis function for surfaces of arbitrary shape, was not presented. Therefore, a full establishment of the surface basis functions of EEM for the surface integral equation as reported in this paper is necessary in the study of electromagnetic scatterings from general targets.

A novel edge-based MoM involving only one triangular patch is proposed for surfaces of any arbitrary shape. It is derived according to the geometrical properties of a local triangle as described in section 1. The combined field integral equations (CFIE) including the electrical field and magnetic field integral equations are presented in section 2. The proposed method is implemented for discretizing the CFIE. Finally, the method is used to compute the scattering field and the results are then compared and validated using those obtained from FE-BE methods.

1 Surface Edge Element Method

1.1 Surface basis function

Suppose an arbitrary point $P(x, y, z)$ shown in Fig. 1 is located inside a triangular patch $\triangle P_1P_2P_3$ on the surfaces of a general object without any of its sides parallel to the X, Y or Z axis. The nodal basis function

Received 2004-08-26.

Foundation item: The National Natural Science Foundation of China (No. 59707003).

Biography: Yu Haitao (1965—), male, doctor, professor, htyu@seu.edu.cn.

in this case is a linear function of coordinates of $P(x, y, z)$,

$$\lambda_{si} = a_i + b_i x + c_i y + d_i z \tag{1}$$

where a_i, b_i, c_i and d_i are coefficients related to the size and shape of the triangle.

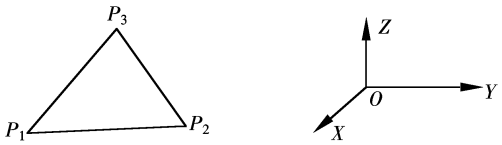

Fig. 1 A triangular patch

According to the properties of nodal basis functions, we can get the following equation:

$$\begin{bmatrix} 1 & x_1 & y_1 & z_1 \\ 1 & x_2 & y_2 & z_2 \\ 1 & x_3 & y_3 & z_3 \\ 0 & n_x & n_y & n_z \end{bmatrix} \begin{Bmatrix} a_i \\ b_i \\ c_i \\ d_i \end{Bmatrix} = \begin{Bmatrix} k_{i1} \\ k_{i2} \\ k_{i3} \\ 0 \end{Bmatrix} \tag{2}$$

where n_x, n_y and n_z are the three normalized components of a normal vector $\boldsymbol{n}$ of the plane $\triangle P_1P_2P_3$, and $K_{ij} = 0$ if $i \neq j$, and $K_{ij} = 1$ if $i = j$. The first three rows of Eq. (2) are obtained according to the properties of nodal basis functions. The fourth row of Eq. (2) is obtained from the geometrical property of a nodal basis function which is equivalent to the normalized plane equation enclosing the corresponding edge on a triangular patch. However, there are many such planes and hence the fourth row in Eq. (2) is imposed to select the plane that is vertical to the local triangle patch as the basis plane, for which Eq. (1) has a unique solution.

Therefore, one of the edge based basis functions related to edge $e = \{i, j\}$ is obtained as follows:

$$\boldsymbol{N}_{se} = \lambda_{si} \nabla \lambda_{sj} - \lambda_{sj} \nabla \lambda_{si} \tag{3}$$

Like the volume edge elements, the following identity is always held,

$$\boldsymbol{N}_{se} \cdot \overline{ij} \equiv \pm 1 \tag{4}$$

which makes sure that the tangential components of the vectors are continuous between two adjacent elements.

The equivalent electrical and magnetic currents related to the tangential magnetic and electric fields on the surface integration are written as

$$\boldsymbol{J}_s = \sum_{e=1}^{3} \boldsymbol{J}_{se} = \sum_{e=1}^{3} \boldsymbol{n} \times \boldsymbol{H}_e = \sum_{e=1}^{3} \boldsymbol{n} \times \boldsymbol{N}_{se} H_e \tag{5}$$

$$\boldsymbol{M}_s = \sum_{e=1}^{3} \boldsymbol{M}_{se} = -\sum_{e=1}^{3} \boldsymbol{n} \times \boldsymbol{E}_e = -\sum_{e=1}^{3} \boldsymbol{n} \times \boldsymbol{N}_{se} E_e \tag{6}$$

where H_e is an edge variable corresponding to the magnetic density, and E_e is the equivalent electric field. $\boldsymbol{n} \times \boldsymbol{N}_{se}$ is a constant in a normal direction to the edge $\overline{ij}$ such that the equivalent currents are continuous in the normal direction of the adjacent elements to satisfy the surface current properties.

The surface charge densities related to the divergences of the surface currents are expressed using surface EEM as follows:

$$\nabla \cdot \boldsymbol{J}_s = 2 \sum_{e=1}^{3} \boldsymbol{n} \cdot (\nabla \lambda_{sj} \times \nabla \lambda_{si}) H_e \tag{7}$$

$$\nabla \cdot \boldsymbol{M}_s = -2 \sum_{e=1}^{3} \boldsymbol{n} \cdot (\nabla \lambda_{sj} \times \nabla \lambda_{si}) E_e \tag{8}$$

For the fundamental EEM, $\boldsymbol{n} \cdot (\nabla \lambda_{sj} \times \nabla \lambda_{si})$ is a constant and therefore, the divergence of current keeps the same value on a triangular patch because of the low order interpolation of the EEM.

1.2 High order surface EEM

In order to improve the accuracy of the numerical solutions, a high order EEM for surfaces of arbitrary shape is necessary. The advantage of Eq. (3) over the RWG function is that the proposed method can be developed into high order methods since the format of Eq. (1) is the same as that of the general expressions of nodal basis functions. The high order edge element still retains the features of the fundamental EEM and overcomes the drawback that the divergence of the vector field is always zero. High order EEM is described in Ref. [11] and hence one can obtain high order surface edge elements readily.

2 Combined Field Integral Equations

Considering Fig. 2, the regions Ω_1 and Ω_2 are characterized by the medium parameters $(\varepsilon_1, \mu_1, \sigma_1)$ and $(\varepsilon_2, \mu_2, \sigma_2)$, respectively. According to surface equivalence principles, the total fields $(\boldsymbol{E}, \boldsymbol{H})$ are determined by a set of equivalent electric and magnetic surface currents. The combined field integral equations for the scattering field from the dielectric and lossy targets are expressed, respectively, as

$$\boldsymbol{E}_{\tan}^{\text{inc}}(\boldsymbol{r}) = \left[\sum_{k=1}^{2} (\mathrm{j}\omega \boldsymbol{A}_k(\boldsymbol{r}) + \nabla \Phi_{ek}(\boldsymbol{r})) \right]_{\tan} + \left[\nabla \times \sum_{k=1}^{2} \frac{F_k(\boldsymbol{r})}{\sigma_k + \mathrm{j}\omega\varepsilon_k} \right]_{\tan} \tag{9}$$

$$\boldsymbol{H}_{\tan}^{\text{inc}}(\boldsymbol{r}) = \left[\sum_{k=1}^{2} (\mathrm{j}\omega \boldsymbol{F}_k(r) + \nabla \Phi_{mk}(\boldsymbol{r})) \right]_{\tan} - \left[\nabla \times \sum_{k=1}^{2} \frac{\boldsymbol{A}_k(\boldsymbol{r})}{\mu_k} \right]_{\tan} \tag{10}$$

where $\boldsymbol{H}_{\tan}^{\text{inc}}(\boldsymbol{r})$, $\boldsymbol{E}_{\tan}^{\text{inc}}(\boldsymbol{r})$ represent the tangential components of the incident fields. Here $\boldsymbol{F}_k(\boldsymbol{r})$ and $\boldsymbol{A}_k(\boldsymbol{r})$ are the electric and magnetic vector potentials, and $\Phi_{ek}(\boldsymbol{r})$ and $\Phi_{mk}(\boldsymbol{r})$ are the electric and magnetic scalar potentials as well.

The surface of homogenous targets is subdivided

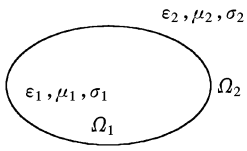

Fig. 2 General geometry for MoM solution

into triangular patches. The computation to the whole region becomes the integral on each small element.

Applying the Galerkin method to Eqs. (9) and (10) and choosing the surface basis function as the weighing function, one gets the dual integrals on the source and field triangular patches. The expressions corresponding to the vector and scalar potentials are expressed as

$$A_{ij}^{k} = \mu_k \iint_{S_i} \boldsymbol{n} \times \boldsymbol{N}_{si} \mathrm{d}S \iint_{S_j} G(\boldsymbol{r}, \boldsymbol{r}') \boldsymbol{J}_s(\boldsymbol{r}') \mathrm{d}S' \tag{11}$$

$$F_{ij}^{k} = \frac{\sigma_k + \mathrm{j}\omega\varepsilon_k}{\mathrm{j}\omega} \iint_{S_i} \boldsymbol{n} \times \boldsymbol{N}_{si} \mathrm{d}S \iint_{S_j} G_k(\boldsymbol{r}, \boldsymbol{r}') \boldsymbol{M}_s(\boldsymbol{r}') \mathrm{d}S' \tag{12}$$

$$\varphi_{e_{ij}}^{k} = \iint_{S_i} \boldsymbol{n} \times \boldsymbol{N}_{si} \cdot \nabla \Phi_{e_{ij}}(\boldsymbol{r}) \mathrm{d}S = \frac{-1}{\sigma_k + \mathrm{j}\omega\varepsilon_k} \cdot \iint_{S_i} \boldsymbol{n} \times \boldsymbol{N}_{si} \mathrm{d}S \cdot \nabla \iint_{S_j} G_k(\boldsymbol{r}, \boldsymbol{r}') \nabla' \cdot \boldsymbol{J}_s(r') \mathrm{d}S' \tag{13}$$

$$\varphi_{m_{ij}}^{k} = \iint_{S_i} \boldsymbol{n} \times \boldsymbol{N}_{si} \cdot \nabla \Phi_{m_{ij}}(\boldsymbol{r}) \mathrm{d}S = \frac{-1}{\mathrm{j}\omega\mu_k} \cdot \iint_{S_i} \boldsymbol{n} \times \boldsymbol{N}_{si} \mathrm{d}S \cdot \nabla \iint_{S_j} G_k(\boldsymbol{r}, \boldsymbol{r}') \nabla' \cdot \boldsymbol{J}_s(r') \mathrm{d}S' \tag{14}$$

and the Green's function

$$G_k(\boldsymbol{r}, \boldsymbol{r}') = \frac{\mathrm{e}^{-\mathrm{j}k_k |\boldsymbol{r}-\boldsymbol{r}'|}}{4\pi |\boldsymbol{r} - \boldsymbol{r}'|} \tag{15}$$

with $k_k = \sqrt{\omega^2 \varepsilon_k \mu_k - \mathrm{j}\omega\mu_k\sigma_k}$ and the subscript $k = 1, 2$ for the homogeneous interior ($k = 1$) and homogeneous exterior regions ($k = 2$), respectively. The complex wave numbers of the interior and exterior regions are given by k_1 and k_2, and the vectors $\boldsymbol{r}$ and $\boldsymbol{r}'$ represent observation and source points, respectively.

The integrals of the incident fields on the field point triangle are expressed as

$$B_{hi} = \iint_{S_i} \boldsymbol{n} \times \boldsymbol{N}_{si} \cdot \boldsymbol{H}^{\mathrm{inc}}(\boldsymbol{r}) \mathrm{d}S \tag{16}$$

$$B_{ei} = \iint_{S_i} \boldsymbol{n} \times \boldsymbol{E}^{\mathrm{inc}}(\boldsymbol{r}) \mathrm{d}S \tag{17}$$

We need to consider the singularity problems about $1/R$ and $\nabla(1/R)$ where $R = |\boldsymbol{r} - \boldsymbol{r}'|$, and analytic expressions must be used on integrals on both the source and field triangles when the two points are located at the same triangle. If the distance between the source and field points is less than half of one wavelength, one needs to use the 3-point or 7-point Gaussian quadrature to approximate the integrals. However the computational speed will decrease greatly as the Gaussian quadrature points increase, therefore one has to use different approximation methods according to the individual situation.

Applying the proposed surface basis functions and current expressions to Eqs. (11) to (15), one can get linear and complex equations as

$$\boldsymbol{K}_{ij} \begin{Bmatrix} H_j \\ E_j \end{Bmatrix} = \{B_j\} \tag{18}$$

where $\boldsymbol{K}_{ij}$ is the impedance matrix and the right hand can be obtained from Eqs. (16) and (17).

The impedance matrix $\boldsymbol{K}_{ij}$ is full. The preconditioned bi-conjugate gradient method is implemented in the computation of the numerical solutions.

3 Numerical Examples

In this section, numerical results are presented for the scattering field under plane wave illumination using the proposed method.

3.1 A dielectric cube

The first example considered here is the plane wave scattering from a dielectric cube, 20 cm on each side. The incident field is 1 V/m coming through the Z axis at a radar frequency of 300 MHz. The proposed edge-based MoM is implemented to compute the scattering field at 100 m away from the center of the target.

Tab. 1 shows the numerical results with different meshes ranging from 12 to 192 triangles, which are obtained using the edge-based MoM. The permittivity of the cube is $\varepsilon_r = 9.0$ and $\sigma = 0$. The computational results at $\theta = 0°$ are convergent and are close to 1 mV/m when the meshes are increased. From Tab. 1, it can be seen that the numerical errors are less than 4% once the edge size of the triangles is less than 0.1 wavelength.

Fig. 3 shows the scattering electric field on the

Tab. 1 Comparison of scattering electricalfield

Number of Triangles	Scattering electric field/(mV·m^{-1})
12	0.795 0
48	0.963 0
108	0.982 0
192	0.989 8
300	0.994 0

XOZ plane with the angle θ varying from 0° to 360° with a test radius $r = 100$ m. The permittivity here is $\varepsilon_r = 4.0$ and the conductivity is $\sigma = 0$. The geometry of the cube is subdivided into 48 triangles with 27 nodes on its surfaces. There are 70 edges on the surfaces. For comparison, the numerical results by FEM-BEM at the same triangles on the surface are also presented.

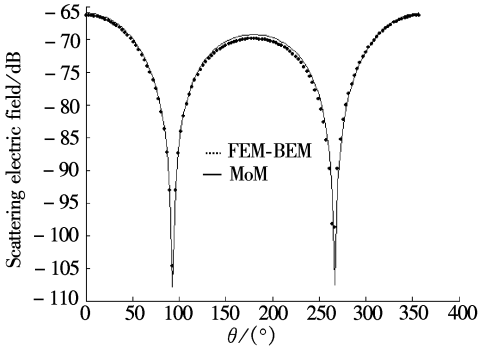

Fig. 3 Scattering field with $\varepsilon_r = 4.0$ and $\sigma = 0$

Fig. 4 shows the scattering electric field on the *YOZ* plane starting at the *Z* axis with the angle φ varying from 0° to 180° with a test radius $r = 100$ m. The conductivity $\sigma = 0.02$ S/m, and the permittivity and meshes here are the same as that in Fig. 3. FEM-BEM results are also used for comparison.

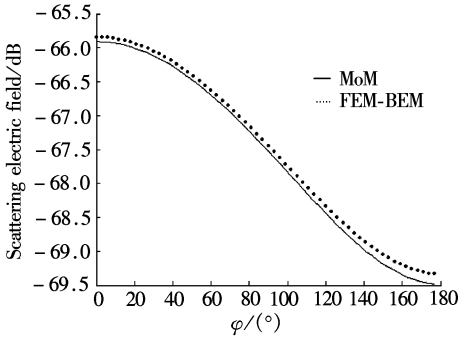

Fig. 4 Scattering field with $\varepsilon_r = 4.0$ and $\sigma = 0.02$ S/m

For a homogenous target, the MoM is superior than FEM-BEM since only the surfaces of the target are meshed using the former while the whole target is required to be subdivided into tetrahedrons for the latter. Therefore, relatively fewer unknowns are required using the proposed MoM.

3.2 A dielectric cylinder

The second example of MoM application is to compute the scattering field from a dielectric cylinder, 2.54 cm in both diameter and length with $\varepsilon_r = 9.0$ and $\sigma = 0.01$ S/m. The cylinder is subdivided into 48 triangles. Results shown in Fig. 5 are computed by using the proposed MoM and then compared with those from FEM-BEM.

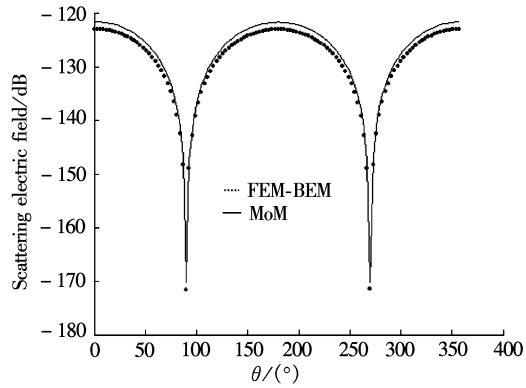

Fig. 5 Scattering electric field by MoM and FEM-BEM

4 Conclusion

The new edge-based MoM in the present work is robust and flexible to use in the computation. Results for solving the scattering field have been given in several cases of dielectrics. The surface edge element method keeps the same features as those of the volume edge elements and can easily be developed into high order elements since the format of surface element method is the same as that of normal edge elements. Results show that scattering field is convergent, and accurate solutions are obtained without using many unknowns. Finally, the numerical results obtained by the proposed method are compared and validated by those from FEM-BEM.

References

[1] Rao S M, Wilton D R, Glisson A W. Electromagnetic scattering by surfaces of arbitrary shape [J]. *IEEE Transactions on Antennas and Propagation*, 1982, **30**(3): 409 − 418.

[2] Bunger R, Beyer R, Arndt F. Rigorous combined mode-matching integral equation analysis of horn antennas with arbitrary cross section [J]. *IEEE Transactions on Antennas and Propagation*, 1999, **47**(2): 1641 − 1648.

[3] Liu Zhijun, Chew Weng Cho, Michielssen E. Numerical modeling of dielectric-resonator antennas in a complex environment using the method of moments [J]. *IEEE Transactions on Antennas and Propagation*, 2002, **50**(1): 1 − 20.

[4] Sheng X Q, Jin J M, Song J M. On the formulation of hybrid finite-element and boundary integral methods for 3-D scattering [J]. *IEEE Transactions on Antennas and Propagation*, 1998, **46**(3): 303 − 311.

[5] Zhang Yunhua, Cui Tiejun, Chew Weng Cho, et al. Magnetic field integral equation at very low frequencies [J]. *IEEE Transactions on Antennas and Propagation*, 2003, **51**(8): 1864 − 1871.

[6] Sarkar T K, Lee Wonwoo, Rao S M. Analysis of transient

scattering from composite arbitrarily shaped complex structures [J]. *IEEE Transactions on Antennas and Propagation*, 2000, **48** (10): 1625 – 1634.

[7] Nedelec J C. Mixed finite element in R^3 [J]. *Numer Math*, 1980, **35** (2): 315 – 341.

[8] Bossavit A. A rational for edge elements in 3-D field computations [J]. *IEEE Transactions on Magnetics*, 1988, **24** (1): 74 – 79.

[9] Ahn C H, Jeong B S, Lee S Y. Efficient vectorial hybrid FE-BE method for electromagnetic scattering problem [J]. *IEEE Transactions on Magnetics*, 1994, **30** (5): 3136 – 3139.

[10] Wakao S, Onuki T. Electromagnetic field computations by the hybrid FE-BE method using edge elements [J]. *IEEE Transactions on Magnetics*, 1993, **28** (2): 1487 – 1490.

[11] Webb J P. Hierarchal vector basis functions of arbitrary order for triangular and tetrahedral finite elements [J]. *IEEE Transactions on Antennas and Propagation*, 1999, **47** (8): 1244 – 1253.

表面棱边单元法求解三维电磁场问题

余海涛

(东南大学电气工程系, 南京 210096)

摘要: 提出了表面棱边单元方法并应用它求解任意形状物体的三维电磁场散色问题. 首先根据物体剖分得出表面区域的几何特性, 推导出表面棱边单元法的基本公式. 该方法保持了普通棱边单元法的基本特性, 维持变量的切向分量连续. 然后用复合积分方程来模拟普通介质的电磁场散色问题, 应用所提出的方法离散积分方程, 并且对奇点问题采用特殊的处理方法. 最后用该方法计算圆柱体以及四方体的在不同介质条件下的电磁场散色问题, 对所得的数值解进行测试, 并与其他数值方法解相比较, 结果表明该方法行之有效.

关键词: 表面棱边单元法; 矩量法; 复合场积分方程; 散色场

中图分类号: TM154